INSTITUTE OF PHYSICS PUBLISHING JOURNAL OF MICROMECHANICS AND MICROENGINEERING

J. Micromech. Microeng. **14** (2004) 462–470 PII: S0960-1317(04)66791-X

A low-power resonant micromachined compass

Thierry C Leïchlé[1], Martin Von Arx[1], Stephen Reiman[2], Iulica Zana[1], Wenjing Ye[2] and Mark G Allen[1]

[1] School of Electrical and Computer Engineering, Georgia Institute of Technology, Atlanta, GA 30332, USA
[2] School of Mechanical Engineering, Georgia Institute of Technology, Atlanta, GA 30332, USA

Received 30 July 2003
Published 9 January 2004
Online at stacks.iop.org/JMM/14/462 (DOI: 10.1088/0960-1317/14/4/005)

Abstract
This paper describes a micromachined magnetic field sensor based on magnetic resonant structures. A micromechanical resonator fabricated using surface micromachining techniques is modified so as to incorporate a magnetic material. The shift of the fundamental mechanical resonant frequency of the device, caused by the interaction of the external magnetic field and the magnetic component of the resonant system, is used to determine the amplitude or the direction of the external field. We have designed, fabricated and tested two types of micromachined magnetic field sensors relying on the proposed principle of operation. The fabrication of the sensors follows CMOS-compatible and low temperature processes based on surface micromachining. Devices have been fabricated which exhibit a minimum resolution of 45° at 30 μT or less, at an excitation voltage of 10 V, demonstrating their utility as a magnetic compass. The power consumed to actuate the resonator is on the order of 20 nW. A theoretical model of the magnetic field sensor was developed using vibration analysis and nonlinear deflection theory. Good agreement was observed between the predicted and observed behavior of the compass.

1. Introduction

A magnetic sensor suitable for an application such as an electronic compass in a wristwatch must fulfill precise requirements. Resolution necessary for navigational use must be on the order of magnitude of the Earth's magnetic field. The magnitude of the Earth's magnetic field varies from about 60 μT near the poles to 30 μT near the equator. Portable applications require small dimensions (millimeter scale), high integration and low power consumption. The power consumption of the micro compass should be on the same order of magnitude as that of a wristwatch, which operating for three years on a 309 battery (voltage of 1.55 V and typical capacity of 80 mAh) consumes 4.5 μW.

A large number of magnetic sensors can be found in the literature. Search coil, flux gate, magnetoresistive and semiconductor-based magnetometers are among the candidate sensors of medium to high sensitivity for portable applications. Semiconductor-based magnetometers, such as Hall-effect sensors, magnetotransistors and magnetodiodes, while light, small and compatible with microelectronics exhibit limited sensitivity [1]. Hall-effect sensors can possess noise and offset issues [2], requiring relatively large power consumption to attain high sensitivity. A monolithic silicon magnetic compass, using two Hall-effect sensors, is reported in [3]. That work successfully demonstrated the integration of the Hall-effect sensors with electronics, but no experiments were carried out for applied magnetic fields lower than 40 mT. Magnetoresistive sensors have high sensitivity at low fields, but the sensitivity scales down with power because of a linear dependence on the drive voltage [4]. An alternative approach, based on the use of a magnetoresistive material mounted on a piezoresistive material is presented in [5]. Excellent device performance (resolution of 0.5 nT) is obtained for a power consumption of a few mW.

The realization of very small search coil and micromachined flux gate magnetometers is usually a challenge because of the difficulty in fabrication of miniaturized coils.

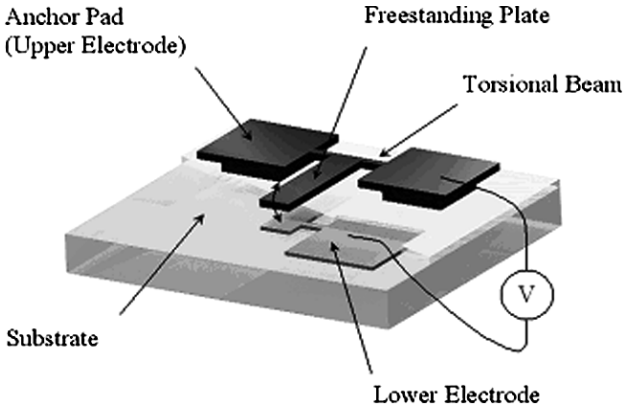

Figure 1. Schematic of the parallel plate resonator.

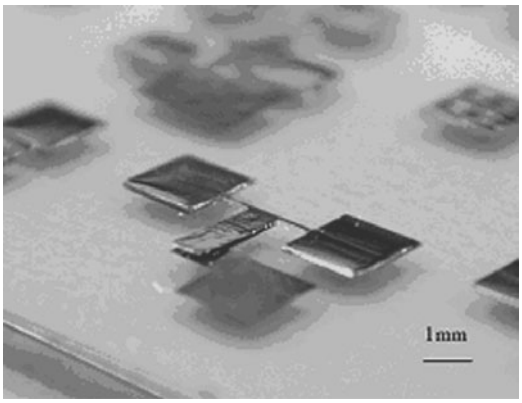

Figure 2. Image of a single Ni–Fe resonator fabricated on a glass substrate. Typical dimensions for the microstructures are 13 μm thickness, 600 μm beam length, 200 μm beam width, 800 μm plate width and 3400 μm plate length.

However, owing to the use of micromachining technology, miniature coils are achievable, and flux gate magnetometers have been realized [6]. Despite a resolution of 0.1 nT, the sensors consume significant levels of power (hundreds of mW) in operation.

Several Lorentz force based magnetometers can be found in the literature [7–9]. Those devices consist of a resonating structure incorporating electrically conductive lines. Drive of the resonator is achieved by the Lorentz force generated by a sinusoidal current flowing through the conductive lines in the presence of a magnetic field. The magnetic field amplitude is deduced from the measurement of the amplitude of vibration. Resolution as low as several nT have been reported, again at the expense of relatively high power consumption.

Two approaches that could lead to low power sensors with high resolution have been recently presented in [4, 10]. By using a permanent magnet on a micro-movable structure to sense the external magnetic field, Judy *et al* [4] predict an integrated sensor that could detect 100 pT and consume less than 1 mW. In [10], a magnetometer based on the magnetoimpedance effect could exhibit a resolution of few nT with less than 1 mW of power.

We propose an alternative approach, using micromachining techniques to build electrostatically driven resonators incorporating magnetic materials, which allow for low power consumption, medium sensitivity, batch fabrication and the potential for readout electronics integration [11, 12]. The micromachined compass consists of a magnetic material suspended on a small resonant structure. The interaction of the magnetic material with an external magnetic field alters the resonant frequency of the microresonator, thereby allowing the readout of the direction of the external field.

2. Proof-of-concept sensor

A first generation of micromachined magnetic field sensors, based on the use of a Permalloy parallel plate resonator, has been fabricated and tested to demonstrate the concept of the sensing mechanism [11]. The main design criterion of the device is a short and simple fabrication process. A conceptual view of the device is shown in figure 1. It consists of a freestanding plate attached to two anchor pads by means of two beams. This resonating structure is made of a soft magnetic material (Permalloy, $Ni_{80}Fe_{20}$ alloy) and is driven into oscillation by means of an applied voltage, which results in an oscillatory electrostatic force on the plate. By applying an ac, superposed with a dc, voltage, frequency-doubling effects resulting from the electrostatic drive can be suppressed. Variation of the frequency of the drive voltage until the amplitude of the vibration of the plate is a maximum results in determination of the resonant frequency of the system. Detection of the maximum amplitude of the plate is extracted from the measurement of the capacitance between the parallel plate and the lower electrode.

The natural frequency of the system depends on the torque produced by the interaction between the magnetization of the plate and the external magnetic field. Hence, the direction of the external magnetic field is determined from the measurement of the resonant frequency of the device. The fabrication process of the device is greatly simplified by making the resonant structure in nickel–iron alloy that exhibits good mechanical and magnetic properties [13, 14]. The fabrication of the Permalloy parallel plate resonator is based on surface micromachining techniques. The structure is created by electroplating copper and nickel–iron in a polymer micromold. The fabrication process starts with the deposition of a 30 nm titanium/200 nm aluminum layer on a glass substrate. This metal layer is patterned using photolithography and is wet etched to create the bottom electrode. An insulator (10 μm of PI2611 polyimide) is then spun and cured on top of the electrodes. A seed layer of 20 nm titanium/300 nm copper is evaporated on top of the polymer. Photoresist (AZ 4620) is then spun and processed to create a 30 μm thick mold. A 5 μm thick copper layer is first electrodeposited in the mold as a sacrificial layer. A 13 μm thick Ni:Fe(80:20 at%) magnetic alloy is electroplated on top of the copper to create the magnetic resonant structure. The photoresist mold is dissolved and the copper sacrificial layer is then selectively and isotropically removed. Since the pads and anchors of the device are larger than the support beams or the resonating portion, no patterning of the sacrificial layer is required as long as the wet etch is stopped as soon as the moving plate is released. The glass substrate is then optionally diced and the devices are tested. Figure 2 shows a photomicrograph of fabricated devices.

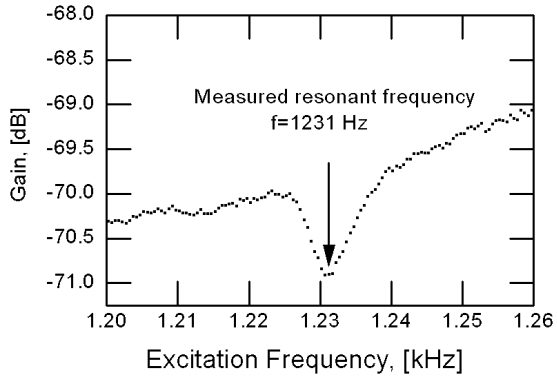

Figure 3. Measured gain of the circuit (shown in figure 4) as a function of the frequency of the actuating signal.

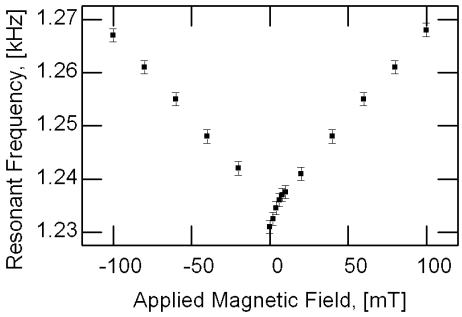

Figure 4. Resonant frequency of the sensor as a function of the magnetic field intensity (magnetic field direction is parallel to the long axis of the free standing plate—see figure 1).

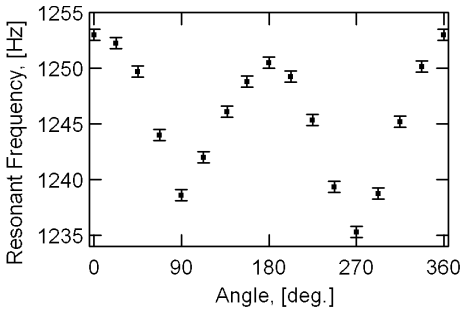

Figure 5. Resonant frequency of the sensor as a function of the direction of the magnetic field (the intensity of the field is 50 mT). Angular orientations of 0 and 180° indicate that the applied magnetic field is parallel to the long axis of the free standing plate—see figure 1.

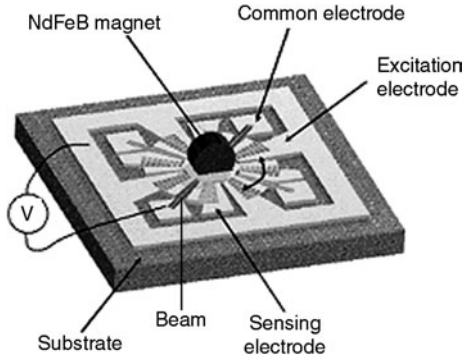

Figure 6. Schematic of the micromachined magnetic compass with a NdFeB permanent magnet.

An HP4194A gain-phase analyzer with associated external circuitry was used to extract the resonant frequency of the sensor. Figure 3 shows a typical output of the gain measurement as a function of frequency under zero applied magnetic field. The measured resonant frequency of the device is 1231 Hz. For magnetic sensing assessment, the device was placed inside an electromagnet that generated the magnetic field in the plane of the resonator. The intensity of the magnetic field, as well as the rotational angle of the sensor relative to the field, could be varied. The applied magnetic field was independently measured by means of a Hall probe integral to the electromagnet. The resonant frequency was then measured as a function of the incident magnetic field amplitude and direction.

Figure 4 shows the variation of the resonant frequency of the device as a function of the applied magnetic field when the direction of the field is parallel to the plate. As expected, due to the symmetry of the device, an absolute-value type response is seen, with minimum resonant frequency at the point of zero applied magnetic field. Resolutions of 2 mT in amplitude of the field have been achieved. The dependence of the resonant frequency on the rotational angle between the applied magnetic field and the device was also studied, and is given in figure 5 for a magnetic field excitation of 50 mT. An angular resolution of 20° in the direction of the field has been achieved.

Although this simple proof-of-concept device has demonstrated that the resonant principle of magnetic field sensing is appropriate on the microscale, it did not achieve the resolution required for use as a micromachined magnetic compass. This motivated the design of a more advanced sensor, incorporating a permanent magnet, as described in the next section.

3. Resonant magnetic field sensor: theory of operation

Figure 6 shows a schematic of the proposed device, which consists of a rotating comb-drive resonator supporting a permanent magnet. The comb-drive resonator is actuated electrostatically into torsional motion. Differential capacitive sensing using a set of sensing electrodes, as well as measurement of the current flowing through the excitation electrodes, can be used for electrical detection. For verification of operation, optical detection can be achieved by observing the fingers' motion under a microscope. The natural frequency of the resonator is a function of the torque produced by the interaction between the magnetization of the permanent magnet and the external magnetic field. Hence, the principle of operation of this device is similar to the concept used for the Permalloy parallel plate sensor, for which the determination of the direction of the magnetic field results from the measurement of the fundamental frequency of the system.

3.1. Fundamental resonant frequency of the comb-drive resonator

The resonator can be simplified to a torsional vibratory system with one degree of freedom, shown in figure 7. The differential

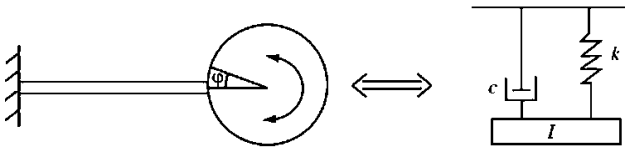

Figure 7. Schematic of a single degree of freedom torsional vibratory system (left) and its equivalent mechanical model (right).

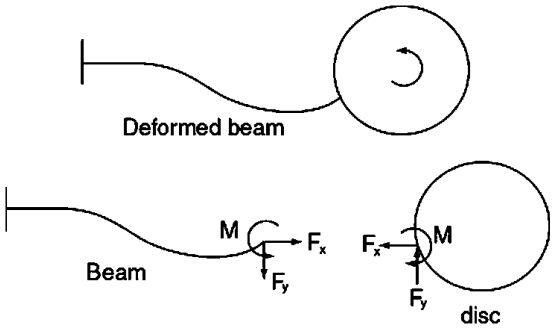

Figure 8. Deformed beam and free body diagrams.

equation describing the motion of the resonator is obtained by summing the moments acting on the resonator (disk). At small oscillation, this equation is

$$I\ddot{\varphi} + c\dot{\varphi} + 4k\varphi = T(t), \tag{1}$$

where I is the mass moment of inertia of the system, k is the stiffness coefficient of one of the four (assumed identical) beams, c is the damping constant and T is an external applied torque. Assuming negligible damping, and no external applied torque, equation (1) becomes

$$I\ddot{\varphi} + 4k\varphi = 0. \tag{2}$$

The solution of this homogeneous linear differential equation with constant coefficients takes the form

$$\varphi = \Phi\, \mathrm{e}^{\mathrm{i}\omega t}, \tag{3}$$

where Φ is the maximum amplitude of the angular deflection, and ω is the natural angular frequency of the system. The fundamental resonant frequency (f) of the resonator is

$$f = \frac{1}{2\pi}\sqrt{\frac{4k}{I}}. \tag{4}$$

3.2. Stiffness coefficient, k—beam model

Rotation of the disk is accompanied by beam deformation (since both ends of the beam are fixed into the connecting structure) as shown in figure 8. The free body diagrams for both the beam and the disk are also shown in figure 8. According to this figure, the torque exerted on the disk due to the beams is

$$T_{\text{beam}} = 4 \times (F_x \times R\sin\varphi + F_y \times R\cos\varphi + M), \tag{5}$$

where F_x, F_y and M are forces in the x- and y-directions and moment respectively, and R is the radius of the disk. Although analytical derivations of F_x, F_y and M are possible, ANSYS finite element analysis is used in this work to extract the relationships between F_x, F_y and M as a function of the rotational angle φ. These quantities are expressed first as functions of δ, the vertical displacement (y-direction) of the tip of the beam. By substituting $\delta = R\sin\varphi$ into those functions, the relationships of F_x, F_y and M with φ are established. Displacement boundary conditions corresponding to different rotational angles (φ) of the disk are prescribed. Curve fitting is then performed to obtain the following equations:

$$F_x = -3 \times 10^{10}\delta^3 + 6 \times 10^6\delta^2 - 0.3148\delta \tag{6}$$

$$F_y = 3 \times 10^9\delta^3 + 8399.1\delta^2 + 0.8682\delta \tag{7}$$

$$M = 1 \times 10^6\delta^3 + 10.938\delta^2 + 0.0012\delta. \tag{8}$$

At small oscillation, the contributions to the torque due to F_x, and nonlinear terms in F_y and M are negligible. Beams behave linearly and the stiffness coefficient (linear) of one beam is $k = 2.068 \times 10^{-6}\ \mathrm{N\,m^{-1}}$.

3.3. Moment of inertia, I

The mass moment of inertia of the resonator is obtained by adding the mass moment of inertia of the central disk, the mass moment of inertia of the cylindrical sections supporting the comb-drive fingers, and the mass moment of inertia due to the moving fingers. The mass moment of inertia due to the beams is of two orders of magnitude lower than the contributions due to the disk and thus is neglected. The expression of the mass moment of inertia is obtained from [15]:

$$I = \rho_{\mathrm{e}} t_{\mathrm{e}} \left(\frac{\pi R^4}{2} + \frac{\pi(r^4 - R^4)}{10}\right) + I_{\mathrm{f}}, \tag{9}$$

in which ρ_{e} is the density of the epoxy, r is the radius of the cylindrical sections and I_{f} is the moment of inertia due to fingers. When adding a cylindrical magnet of thickness t_{m}, radius r_{m} and density ρ_{m} on the epoxy resonator, the moment of inertia of the system becomes

$$I = \pi\rho_{\mathrm{e}} t_{\mathrm{e}} \left(\frac{4R^4 + r^4}{10}\right) + I_{\mathrm{f}} + \left(\frac{\pi\rho_{\mathrm{m}} r_{\mathrm{m}}^2 t_{\mathrm{m}}^3}{12} + \frac{\pi\rho_{\mathrm{m}} r_{\mathrm{m}}^4 t_{\mathrm{m}}}{4}\right). \tag{10}$$

The calculated moment of inertia of the system is $I = 5.17 \times 10^{-12}\ \mathrm{kg\,m^2}$.

3.4. Resonant frequency

The resonant frequency of the resonator is obtained by substituting values of k and I into equation (4). Typical geometry values for the fabricated microstructure, shown in figure 6, and the material properties values for the epoxy and the NdFeB alloy are used. The predicted value is 201 Hz for the complete resonator incorporating a permanent magnet. For model validation, ANSYS analysis was also used to extract the first two resonant modes of the structure and the corresponding resonant frequencies; the ANSYS-predicted fundamental resonant frequency is 209 Hz. The difference in resonant frequency between the theoretical prediction and the ANSYS modal analysis is due to ignoring the moving comb fingers (which contribute to the total moment of inertia) in the ANSYS modal analysis. If the mass moment of inertia due to fingers is ignored in our theoretical analysis, the predicted natural frequency increases from 201 Hz to 211 Hz, which is much closer to the 209 Hz obtained from the ANSYS modal analysis.

3.5. Change of resonant frequency in the presence of a magnetic field

The interaction between an external magnetic field surrounding the sensor and the permanent magnet attached to the resonator produces a torque on the magnet. This torque tends to align the direction of magnetization of the magnet with the direction of the external field. When the direction of magnetization is parallel to the external field, the magnetic torque is zero and the static resonator does not experience any rotation. However, when the resonator is oscillating the torque increases as the rotational resonator is pulled away from its equilibrium position. Assuming small oscillation, the resonant frequency is obtained by summing the moments acting on the system and solving the equation given below:

$$I\ddot{\varphi} + 4k\varphi - T\sin(\theta - \varphi) = 0 \tag{11}$$

where φ is the angle of oscillation, and θ is the angle between the direction of the magnetization (which is fixed with respect to the geometry of the magnet) and the external magnetic field. For simplicity, T, is the amplitude of the magnetic torque, and is given by equation (12) for a magnet of volume V and magnetization M. The expression of the resonant frequency is given by equation (13)

$$T = \mu_0 M V H \tag{12}$$

$$f = \frac{1}{2\pi}\sqrt{\frac{4k + T\cos\theta}{I}}. \tag{13}$$

Hence, when the magnetization and the external field are pointing toward the same direction (i.e., $\theta = 0°$), the device is expected to resonate at a higher resonant frequency than when the magnetization and field vectors are opposite (i.e., $\theta = 180°$).

When the magnetization and the magnetic field are not perfectly aligned (θ is different than 0 or 180°), the resonator rotates due to the magnetic torque produced by the interaction between the external applied magnetic field and the magnetization of the permanent magnet (see figure 9), reaching an equilibrium angle α. This angle is determined by

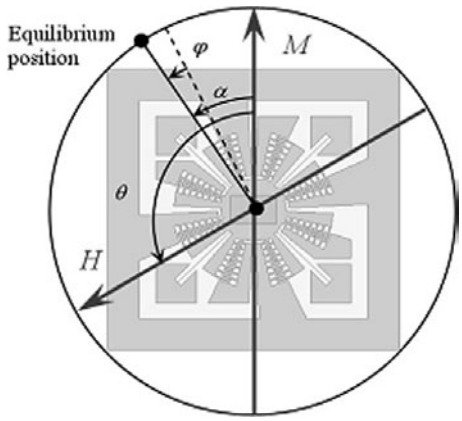

Figure 9. Schematic drawing of the device, including the definition of the angles.

solving the equilibrium equation stating that the sum of the torques acting on the system is zero:

$$4 \times (F_x \times R\sin\alpha + F_y \times R\cos\alpha + M) - T\sin(\theta - \alpha) = 0. \tag{14}$$

Nonlinear effects take place when the equilibrium angle α is away from zero (i.e., the contributions to the torque due to F_x and nonlinear terms in F_y and M become significant). Beams become much stiffer and the resonator oscillating around α exhibits a higher resonant frequency.

The expression of the fundamental resonant frequency of the sensor is obtained by solving the differential equation satisfied by the angle of vibration, φ

$$I\ddot{\varphi} + 4 \times [F_x \times R\sin(\varphi + \alpha) + F_y \times R\cos(\varphi + \alpha) + M] - T\sin(\theta - \alpha - \varphi) = 0. \tag{15}$$

Substituting (6), (7), (8) and $\delta = R\sin(\varphi + \alpha)$ into (15) and assuming small oscillations, i.e., $|\varphi| << 1$, equation (15) can be linearized in terms of φ and the natural frequency can then be obtained.

The change of resonant frequency of the magnetic field sensor with the direction and amplitude of the external magnetic field has been simulated using Matlab. Figure 10(*a*)

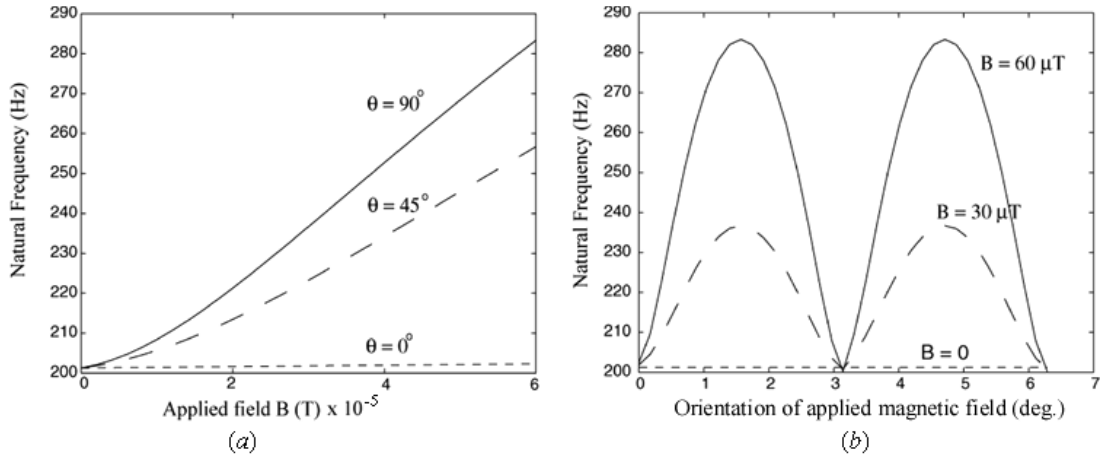

Figure 10. Calculated natural frequency as a function of the (*a*) direction, and (*b*) amplitude of the applied magnetic field.

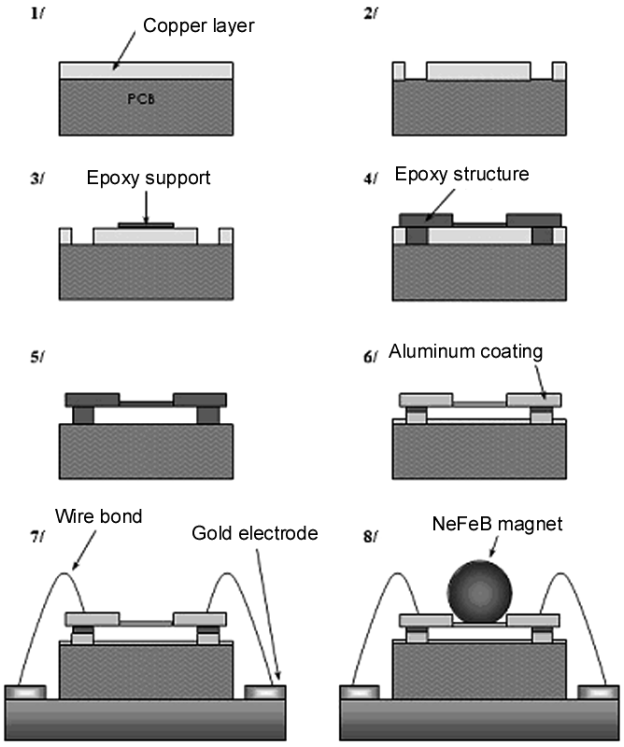

Figure 11. Fabrication process of the compass: (1) polishing of the copper layer; (2) after patterning of the anchor pads; (3) creation of the support for the magnet; (4) fabrication of the epoxy structure; (5) release of the resonator; (6) conformal coating; (7) packaging; (8) mounting of the permanent magnet.

shows the resonant frequency of the sensor versus the amplitude of the magnetic field for different orientations, while figure 10(*b*) shows the variation of the resonant frequency with the direction of the external field, for several amplitudes of the magnetic field.

4. Fabrication and results

For demonstration purposes, SU-8 epoxy has been selected for the resonant structure because of its relatively low modulus of elasticity (resulting in very compliant beams), and the simple fabrication process inherent to its use [16]. Because of its high remanent magnetization, a neodymium–iron–boron (NdFeB) permanent magnet has been chosen to be integrated to the epoxy-based comb-drive resonator in order to realize the micromachined magnetic field sensor.

The details of the fabrication process are shown in figure 11. The substrate is a printed circuit board covered by a polished 70 μm thick copper layer. The copper layer is patterned using conventional positive photoresist and is wet etched to create the anchor points for the resonant epoxy structure. A 10 μm layer of photosensitive epoxy is spun, cured and patterned on top of the copper layer to serve as a mechanical support for the magnet. Another epoxy layer of 140 μm in thickness is processed to create the resonant structure. The dicing of the substrate is done prior to the release of the resonators in order to minimize the risk of device breakage. The copper sacrificial layer is then wet etched to release the suspended parts of the epoxy structures. The

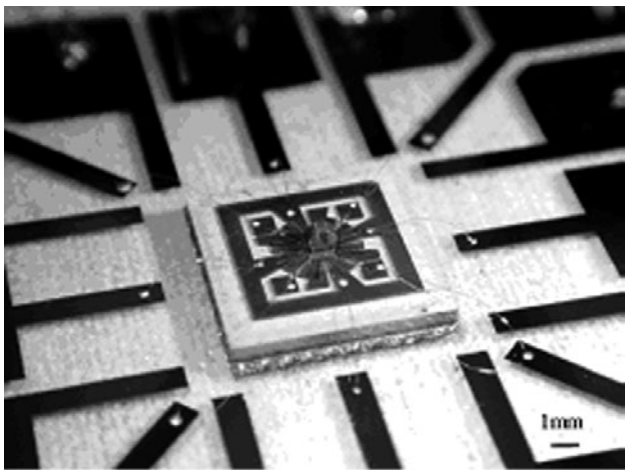

Figure 12. Photograph of a fabricated resonator incorporating a permanent magnet.

resonators are conformally coated with 300 nm of aluminum to create conductive electrodes at the surface of the devices. Shorting due to this conformal coating is prevented due to the undercut of the device anchors.

To facilitate the testing of the sensor, each diced device is glued to a glass substrate, on which gold electrodes were previously patterned. Wire bonds are formed between the resonator's electrodes and the patterned gold on the glass slide. Electrical connection of the device is achieved by making contact on the gold electrodes.

To incorporate the magnetic material, a region in the center of the resonator is formed with a rectangular recess during the previous photolithography steps. A cylindrical N45-grade NdFeB magnet is partially lapped on one side to create a flat region parallel to the thickness direction, and the magnet is adhered flat-side down to the resonator using adhesive. As the base of the cylindrical magnet is perpendicular to the top surface of the structure, the direction of magnetization is in a plane parallel to the plane of rotational motion of the resonator.

Figure 12 shows a completed sensor ready for testing. The typical geometry values for the epoxy structure are 140 μm thickness, 2300 μm beam length, 20 μm beam width, 1000 μm plate inner radius and 2450 μm plate outer radius. The NdFeB magnets are nominally 1600 μm in diameter and 800 μm in thickness.

Measurement of the fundamental resonant frequency of the comb-drive resonator has been achieved both optically and electrically. Comparison between the results given by the two methods was used to validate the accuracy of the measurement methods. The optical measurement consisted of determining the maximum angular deflection of the comb drive with an optical microscope. This method allowed evaluating the natural frequency within 1 Hz. Electrical determination of the resonant frequency was achieved by measuring the intensity of the current flowing through the comb-drive electrodes at the third harmonic of the excitation signal. This was performed in the following manner. The output of the amplifier, delivering the resonator excitation voltage, is connected to the static electrode of the device. The moving electrode is connected to a low-noise current preamplifier SR570 that provides a virtual ground. The amplified current is converted to a voltage and

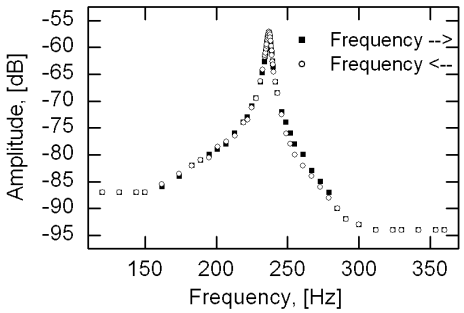

Figure 13. Resonance peak (third harmonic) of a comb-drive resonator incorporating a magnet.

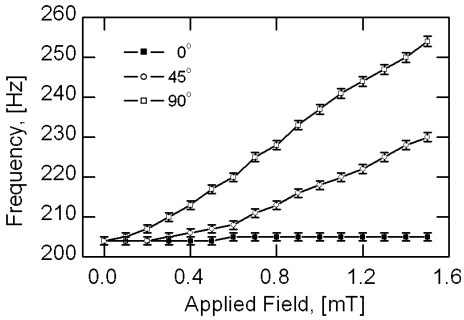

Figure 14. Resonant frequency of the sensor as a function of the applied magnetic field. The angle between the direction of the field and the magnetization is set to 0, 45 and 90°.

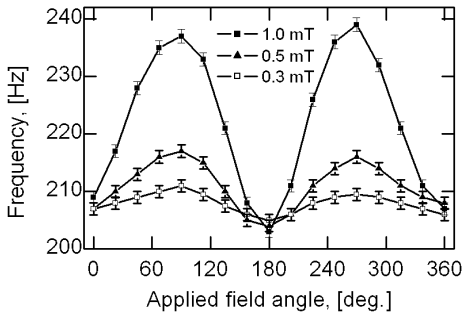

Figure 15. Resonant frequency of the sensor as a function of the direction of the applied magnetic field. An angular orientation of 0° indicates that the applied magnetic field is parallel to the direction of remanent magnetization in the magnet (which is parallel to cylinder's axis). Magnetic field intensity has the values 0.3 mT, 0.5 mT and 1 mT.

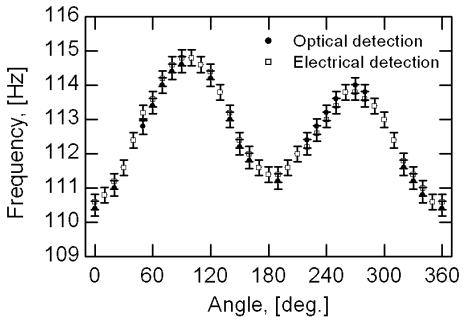

Figure 16. Resonant frequency of a 109 Hz natural frequency sensor as a function of the orientation of the sensor relative to the Earth's magnetic field. No additional external magnetic field is applied.

fed into a spectrum analyzer HP3561A. The spectrum analyzer outputs the Fourier transform of the input signal. The resonant frequency of the particular device has been optically measured to be 238 Hz. As expected, because of the frequency-doubling effects resulting from the ac electrostatic drive, the spectrum consists of peaks at the excitation signal frequency and its harmonics. The third harmonic amplitude of the current is at maximum when the device resonates.

The resonance peak of a fabricated sensor has been obtained by plotting the third harmonic amplitude of the sensing signal as a function of frequency (see figure 13). The amplitude of the driving voltages was 22.5 V and no external magnetic field was applied. A quality factor of approximately 60 was estimated from the plot. A resolution of 0.2 Hz in the determination of the resonant frequency was achieved using this method.

For magnetic sensing assessment, a device with a natural frequency of 205 Hz was placed under a microscope, in the vicinity of a coil that generated a magnetic field in the plane of the resonator. The intensity of the magnetic field was adjusted by varying the current flowing through the coil. The angle of the sensor relative to the field was stepped by rotating the stage of the microscope. The applied magnetic field was independently measured using a gaussmeter (FWBell 9550).

The resonant frequency was measured as a function of the amplitude of the incident magnetic field. Figure 14 shows the variation of the resonant frequency of the device (in Hz) as a function of the applied field (in mT) for different angles between the direction of the field and the magnetization of the permanent magnet. Resonant frequency was determined using the optical method. As the angle increases, and thus the torque produced on the magnet increases, the resonant frequency becomes more sensitive to a change in the magnetic field amplitude.

The dependence of the resonant frequency on the rotational angle between the applied magnetic field and the magnetization was investigated using the same device, and the results are shown in figure 15. The dependence of resonant frequency was plotted for three different values of the magnetic field excitations. As expected, the change of resonant frequency increases with the amplitude of the field.

The behavior of a device exhibiting a lower resonant frequency (109 Hz) and thus expected to be more sensitive was also studied. The resonant frequency was measured by optical and electrical means and the device was excited using an ac signal of 37.5 V. No magnetic field was applied, thus allowing the sensor to determine the direction of the Earth's magnetic field.

Figure 16 shows the dependence of the resonant frequency on the rotational angle. A minimum resolution of 10° in the direction of the field was estimated from the plotted results. Resolution in the amplitude of the field is expected to be well below 30 μT, but is difficult to quantify further from these data. The same experiment was conducted with a lower excitation voltage of 10 V. The sensor could still resolve 45° in the directions of the Earth's magnetic field.

The power consumption of the sensor was estimated from the measurement of both resonator excitation voltage

and resultant displacement current. Typical calculated power consumption at an excitation of 30 V is approximately 0.4 μW.

5. Discussion

The similarity between the shapes of the plots shown in figures 10(*a*) and (*b*), and those shown in figures 14 and 15, respectively, allows us to believe that the theoretical model can account for the experimental results. As predicted by the model, the sensor tested in the previous section exhibits a lower resonant frequency when the angle between the direction of the magnetization and the direction of the external magnetic field is equal to 180° than when it is 0°. The resonant frequency experiences maxima when the direction of the magnetic field is perpendicular to the direction of the magnetization. However, the plot in figure 16 does not reflect the perfect symmetry of the theoretical curve. The two resonant frequency maxima have different values. This is probably due to the observed offset position of the permanent magnet from the axis of symmetry of the epoxy structure. This offset position is due to the non-accurate manual positioning of the magnet on the plate and results in a misalignment of the axis of inertia of the magnet, the direction of the magnetic torque and the axis of rotation of the resonator.

Experimental measurements of natural frequencies at $\theta = 0^\circ$ and $\theta = 180^\circ$ in the case of $B = 0.3$ mT are used to determine the empirical values of the magnitude of the magnetic torque and the stiffness coefficient of the beams. These values will be compared with theoretical predictions. According to (13) and experimental data, we have

$$f(\theta = 0^\circ) = \frac{1}{2\pi}\sqrt{\frac{4k+T}{I}} = 206.8 \tag{16}$$

$$f(\theta = 180^\circ) = \frac{1}{2\pi}\sqrt{\frac{4k-T}{I}} = 205. \tag{17}$$

If the theoretical value of I (equation (11)) is used, the deduced value of the linear stiffness coefficient is 2.165×10^{-6} N m^{-1}, which is very close to the theoretical prediction ($k = 2.068 \times 10^{-6}$ N m^{-1}). However, the deduced magnitude of the magnetic torque is 7.6×10^{-8} N m, which is about four times smaller than the theoretical prediction of 3×10^{-7} N m. This is probably due to the nonuniformities in the magnetization within the permanent magnet volume caused by the demagnetization effects around the magnet edges, cumulated with reasonable oxidization of the surface of the magnet (which would reduce the magnetization), as well as a sizeable damage incurred by the magnet during its preparation for mounting.

The set of equations (16), (17) can also be used to deduce the moment of inertia of the system and the magnitude of the torque by assuming that the theoretical prediction of the linear stiffness coefficient is correct. This gives a moment of inertia of 4.942×10^{-12} kg m^2, which, again, is very close to the theoretical value (5.17×10^{-12} kg m^2), and a magnetic torque of 7.2×10^{-8} N m.

To check consistency, the theoretical prediction of stiffness coefficient, the deduced values of I (4.942×10^{-12} kg m^2) and T ($T = 1.21 \times 10^{-7}$ for $B = 0.5$ mT and $T = 2.42 \times 10^{-7}$ for $B = 1$ mT) obtained from experimental results corresponding to $B = 0.3$ mT are used to predict the natural frequencies at $\theta = 0^\circ$ and $\theta = 180^\circ$ for the cases of $B = 0.5$ mT and $B = 1$ mT. Results, together with experimental data, are shown in table 1. A good agreement has been achieved, indicating consistency in both theoretical analysis and measurements.

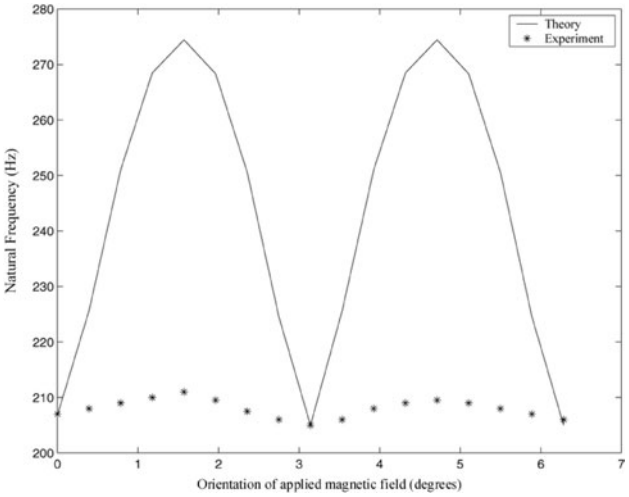

Figure 17. Comparison of resonant frequencies—theory versus experiment, for an applied field of 0.3 mT.

Table 1. Natural frequencies of the resonator at $\theta = 0^\circ$ and $\theta = 180^\circ$.

	$\theta = 0^\circ$		$\theta = 180^\circ$	
B (mT)	Calculated (Hz)	Measured (Hz)	Calculated (Hz)	Measured (Hz)
0.5	207.39	207	204.40	204
1	208.88	209	202.88	203

However, when comparing the amplitude of the theoretical curve (that is, frequency at $\theta = 90^\circ$) with the experimental curve, a large discrepancy has been observed (see figure 17). Since the amplitude of the curve is largely dependent on the nonlinear stiffness coefficients of beams (coefficients corresponding to δ^2 and δ^3 in equations (6), (7), (8)), this indicates weaker nonlinear effects in experiments than they were predicted by the theory. Although further investigations are necessary in order to explain this discrepancy, possible error sources in our beam model are considered to be: (1) idealized 'fixed' ends and (2) neglected effects of residual stress in the epoxy.

6. Conclusions

In this paper, we have successfully fabricated a magnetic field sensor based on an alternative approach using a micromechanical resonator incorporating a magnetic material. The principle of operation of the device relies on its change of resonant frequency caused by the interaction of the external magnetic field and the magnetic material part of the resonant system.

The principle of operation was demonstrated on a soft magnetic resonator, which was fabricated using a simple process. The sensor consists of a Permalloy parallel

plate microstructure driven electrostatically at resonance. Resolution of 2 mT in amplitude of the field was achieved for an excitation voltage of 250 V.

Design optimization led to the second type of micromachined magnetic field sensor. We selected the materials and geometry of the device in order to maximize the torque produced by the external field and to emphasize its effect on the resonant frequency of the system. The resonator is a rotational comb drive, excited electrostatically and the magnetic torque is exerted in the plane of motion of the device. The structure, made of SU-8 epoxy, is easy to fabricate and leads to a very compliant device exhibiting a low resonant frequency (typically between 100 and 200 Hz). The NdFeB permanent magnet (N45 grade), is incorporated manually into the resonator and has a very high remanent magnetization, thus maximizing the effect of the external magnetic field. The device has been successfully demonstrated as an electronic compass, exhibiting a minimum resolution of 45° for an excitation voltage of 10 V. The fabrication process, being CMOS compatible, allows for electronics integration. Using electrostatic excitation, the device has the potential to be of ultra low power consumption, therefore, the limiting factor becoming the power required by the sensing electronic circuitry. The small dimensions of the micromachined resonant magnetic field sensor, its fabrication process, performances and power consumption make it an excellent candidate for portable and medium sensitivity applications.

References

[1] Lenz J E 1990 A review of magnetic sensors *Proc. IEEE* **78** 973–89

[2] Popovic R S, Flanagan J A and Besse P A 1996 The future of magnetic sensors *Sensors Actuators* A **56** 39–55

[3] Maenaka K, Tsukahara M and Nakamura T 1990 Monolithic silicon magnetic compass *Sensors Actuators* A **21–23** 747–50

[4] Judy J W, Yang H, Myung N, Irazoqui-Pastor P, Schwartz M, Nobe K and Yang K 2000 Ferromagnetic micromechanical magnetometers *Solid-State Sensor and Actuator Workshop (Hilton Head Island, SC, USA)* p 15

[5] Lynch B J and Gallantree H R 1990 A new magnetic sensor technology GEC *J. Res.* **8** 13–9

[6] Kawahito S, Sasaki Y, Sato H, Choi S O, Nakamura T and Tadokoro Y 1994 Miniature fluxgate sensing element for high-performance integrated silicon magnetic sensors *Sensors Mater.* **5** 241–51

[7] Wickenden D K, Kistenmacher T J, Osiander R, Ecelberger S A, Givens R B and Murphy J C 1997 Development of miniature magnetometers *John Hopkins APL Technical Digest* **18** 7–11

[8] Kadar Z, Bossche A and Mollinger J 1994 Integrated resonant magnetic-field sensor *Sensors Actuators* A **41–42** 66–9

[9] Donzier E, Lefort O, Spirkovitch S and Bailleu F 1991 Integrated magnetic field sensor *Sensors Actuators* A **25–27** 357–61

[10] Mohri K, Uchiyama T and Panina L V 1997 Recent advances of micro magnetic sensors and sensing application *Sensors Actuators* A **59** 1–8

[11] Leïchlé T C, Von Arx M and Allen M G 2001 A micromachined resonant magnetic field sensor *Proc. IEEE Micro Electro Mechanical Systems (Interlaken, Switzerland)* pp 78–85

[12] Leïchlé T C, Ye W and Allen M G 2003 A sub-μW micromachined magnetic compass *Proc. IEEE Micro Electro Mechanical Systems (Kyoto, Japan)* pp 154–61

[13] Chung C and Allen M G 1996 Measurement of mechanical properties of electroplated nickel - iron alloys *ASME Int. Mechanical Engineering Congress and Exposition* pp 199–204

[14] Taylor W P, Schneider M, Baltes H and Allen M G 1997 Electroplated soft magnetic materials for microsensors and microactuators *Proc. IEEE Transducers (Chicago, IL, USA)* pp 1445–8

[15] Timoshenko S P and Gere J M 1990 *Mechanics of Materials* 3rd edn (Boston, MA: PWS-KENT)

[16] Lorenz H, Despont M, Fahrni N, Brugger J, Vettiger P and Renaud P 1998 High-aspect-ratio, ultrathick, negative-tone near-UV photoresist and its applications for MEMS *Sensors Actuators* A **64** 33–9